

1 *This is a pre-print of a manuscript submitted for publication*

2 **Title:** Influence of floods, tides, and vegetation on sediment retention in Wax Lake Delta, LA,
3 USA

4 **Authors:** E.A. Olliver¹, D.A. Edmonds¹, and J.B. Shaw²

5 ¹Department of Earth and Atmospheric Science, Indiana University, Bloomington, IN, USA

6 ²Department of Geosciences, University of Arkansas, Fayetteville, AR, USA

7 *corresponding author, colliver@indiana.edu

8 **Key Points**

- 9 1. Use numerical modeling to analyze sediment retention on a delta for various flood-wave
10 magnitudes, tidal amplitudes, and vegetation extents
11
12 2. Vertical accretion increases with flood size, but sediment retention decreases, and tides
13 increase retention during large floods
14
15 3. Vegetation reduces accretion and sediment retention on the delta due to the greater
16 influence of buffering effect versus the trapping effect

17 **Abstract**

18 Sediment is the most valuable natural resource for deltaic environments, and to build new land
19 sediment must be retained in the delta instead of being transported offshore. Despite this, we do
20 not know what controls sediment retention within a delta. Here we use a calibrated numerical
21 model of Wax Lake Delta, LA, USA to analyze sediment retention for different flood-wave
22 magnitudes, tidal amplitudes, and vegetation extents. We only model transport of silt since it
23 comprises most of the incoming sediment load. Our results show that as flood size increases,
24 areally-averaged vertical accretion increases from 0.33 cm to 2 cm, but this comes at a cost
25 because delta-scale sediment retention decreases from 72% to 34%. On a fully vegetated delta,
26 we show that the buffering effect of vegetation reduces island-directed sediment flux by 14 to
27 22% because sediment takes the less resistive path in the channel. When sediment gets onto the
28 islands, the trapping effect of vegetation increases retention by ~10%. But, this is not enough to
29 offset the buffering effect, and vegetation decreases vertical accretion and sediment retention

30 across the delta reduces by up to ~ 0.5 cm and 6%, respectively. We suggest that vegetation will
31 increase sedimentation only when trapping compensates for buffering. Finally, greater tidal
32 amplitude at higher discharges enhances vertical accretion by ~ 0.5 cm per flood as compared to a
33 minimum tidal amplitude condition. These results inform how coastal deltaic systems grow and
34 suggest how to operate sediment diversions more efficiently in deltas with reduced sediment
35 supply.

36 **1. Introduction**

37 Sediment retention is a key unknown in the delta building process. Obviously, sediment
38 must be deposited nearshore for delta building to occur, but we know little about what controls
39 how much of the incoming sediment is retained for delta building and how much is transported
40 out of the delta. The simplest way to quantify retention is as the fraction of sediment deposited
41 relative to the total input over a given time interval (Paola et al., 2011). It is critical that we
42 understand the controls on sediment retention because sediment delivery to most deltas is being
43 reduced. For example, on the Mississippi River, the installation of dams has reduced sediment
44 transport downstream and construction of containment levees has limited the overbank flooding
45 and deposition necessary for wetland sustainment (Stanley & Warne, 1993; Syvitski et al., 2005,
46 2007; Yang et al., 2005; Blum & Roberts, 2009; Meade & Moody, 2010). As a result, over the
47 past 80 years this sediment starvation has contributed to the conversion of ~ 5000 km² of land
48 into open water (Couvillion et al., 2011). Given these losses, it has become widely accepted that
49 coastal restoration in Louisiana must focus on maximizing land building and reducing additional
50 land loss. Despite the reduction in sediment loads to the coast, some river systems still transport
51 enough sediment to build new deltaic wetlands, such as the Atchafalaya and Wax Lake deltas
52 within the greater Mississippi River Delta (MRD) (Roberts et al., 2003; Rosen & Xu, 2013;

53 Carle et al., 2015). Thus, a central component of coastal restoration plans in Louisiana is
54 strategic placement and operation of freshwater and sediment diversions, which emulate the
55 natural processes of crevassing and deltaic land building (CPRA, 2017). Crucially, diverting
56 water and sediment into desired areas does not guarantee land building. Land building will only
57 occur when sediment is retained within the delta, and successful diversions should aim to
58 maximize sediment retention.

59 Sediment retention depends on the processes that supply and remove sediment in a
60 deltaic system. We divide these processes into continuous or episodic. The continuous processes
61 include riverine discharge, the presence of vegetation, tides, and waves. Of these continuous
62 processes, field measurements over days to months indicate that riverine discharge is the primary
63 control of sediment delivery to the system, which is important for eventual sediment retention
64 (Fabre, 2012; Day et al., 2016a; Allison et al., 2017; Keogh et al., 2019). Previous work has
65 shown vegetation enhances sediment deposition and retention in both salt marshes and deltaic
66 freshwater marshes by decreasing water flow velocities, enhancing bed roughness, and directly
67 capturing sediment in the vegetation canopy (Leonard & Luther, 1995; Christiansen et al., 2000;
68 Neumeier & Ciavola, 2004; Gedan et al., 2011; Fagherazzi et al., 2012; Nardin & Edmonds,
69 2014; Nardin et al., 2016; Ma et al., 2018; Larsen, 2019). However, in some instances,
70 vegetation has also been shown to act as a buffer, directing the flow of sediment laden water
71 away from vegetated areas (Nardin & Edmonds, 2014; Nardin et al., 2016; Temmerman et al.,
72 2005, 2007).

73 While we have some sense of how water discharge and vegetation influence retention,
74 relatively little is known about waves and tides. In the paired observational and numerical
75 modeling study by Allison et al. (2017), they determined from fluorescent tracers that retention

76 of the riverine sediments in the West Bay receiving basin was more evenly distributed in space
77 than predicted by the modeling results. Allison et al. (2017) suggested this more even
78 distribution could be due to influence of tides, waves, or wind-driven currents. While Allison et
79 al. (2017) did not measure or model tidal processes, there is conjecture that tides maybe
80 important for sediment retention (Hiatt et al., 2019). Analyses of process connectivity in Wax
81 Lake Delta indicates tidal influence is greatest at the delta shoreline and decreases updelta
82 (Sendrowski & Passalacqua, 2017). However, because Wax Lake Delta is relatively small, the
83 tidal influence could be important because it extends further updelta than in a larger, more
84 heterogeneous system like the MRD. The resuspension of sediment by wind-driven waves has
85 been identified as a key process transporting sediment in shallow bays and estuaries in the MRD
86 (Lane et al., 2007; Wang et al., 2018), resulting in sediment transport in and out of deltaic
87 environments. Additionally, edge erosion by waves can result in degradation of existing deltaic
88 marshes (Day et al., 2011; Mariotti, 2016; Ortiz et al., 2017).

89 The aforementioned processes are more or less continuously operating, and there are
90 other episodic processes, such as hurricanes and seasonal cold fronts, that influence sediment
91 retention in the MRD. Southerly and easterly winds of an approaching cold front can result in a
92 net influx of water into coastal bays and wetlands with resulting inundation of 30-50 cm (Denes
93 & Caffrey, 1988; Childers & Day, 1990). Winds shift to westerly and northerly as cold fronts
94 pass, resulting in rapid drainage of the flooded wetlands. The inundation and draining caused by
95 these cold fronts in autumn and winter results in the transport of sediment, nutrients, and organic
96 matter among coastal bays, adjacent wetlands, and the Gulf of Mexico (Madden et al., 1988;
97 Childers & Day, 1990; Stern et al., 1991; Perez et al., 2000). Despite this, the role of cold fronts
98 in building deltaic land is relatively understudied. However, on WLD Bevington et al. (2017)

99 showed that during a winter cold front season, sediment was eroded from the deltaic islands.
100 Large storm surges associated with hurricanes occurring between June and November can result
101 in significant deposition and erosion of wetlands (Turner et al., 2006; Day et al., 2007). For
102 example, Hurricanes Katrina and Rita resulted in the conversion of ~100 km² of wetlands in the
103 Breton Sound Basin to shallow marsh with erosion of more than 1 m in some areas, while other
104 areas saw 5-10 cm of deposition (Day et al., 2007). Numerical simulations of Hurricanes Katrina
105 and Rita and their impact on the WLD indicate wave action produced significant erosion (Xing
106 et al., 2017). Despite the constructive and destructive force of hurricanes, Smith et al. (2015)
107 reported long-term sediment deposition due to hurricanes to be significantly less than what is
108 supplied by fluvial sources.

109 These continuous and episodic processes also vary in time and space, which has an
110 important influence on retention. This means that the retention fraction depends on the temporal
111 and spatial scales. For example, in a study of the West Bay diversion in the MRD, Allison et al.
112 (2017) reported a riverine sand retention of nearly 100% over two weeks. However, this
113 retention rapidly decreased to 40% after multiple months. This decrease in the retention fraction
114 is likely the result of sediment escaping the system at longer time scales (Xu et al., 2019).
115 Similarly, sediment retention should increase when measured over larger spatial scales, but there
116 is no widely agreed upon definition of the seaward boundary for a receiving basin (Xu et al.,
117 2019). On the temporal side, the seasonal and intra-annual variability of water and sediment
118 discharge strongly influences the magnitude of sediment retention for various years or periods of
119 a given year (Day et al., 2016a,b; Peyronnin et al., 2017). On Davis Pond in the MRD, the
120 sediment retention changed from 44% during winter/spring to 81% during summer/fall (Keogh et
121 al., 2019). The lower winter/spring retention fraction likely results from the higher water

122 velocities observed during that period, keeping more sediment in suspension and decreasing
123 water residence over the basin (Keogh et al., 2019). Keogh et al. (2019) also suggested the
124 seasonally variability in vegetation presence likely increased retention from the winter/spring to
125 summer/fall.

126 Despite these studies, we still lack an understanding of how these forcing mechanisms
127 interact to retain sediment within a delta. This knowledge gap is of theoretical and practical
128 importance, because understanding how these forces interact would inform how coastal deltaic
129 systems grow and help operate planned sediment diversions more efficiently. Field-based
130 approaches have illustrated just how variable sediment retention can be in time and space (Fabre,
131 2012; Day et al., 2016a; Allison et al., 2017; Esposito et al., 2017; Keogh et al., 2019), and an
132 important next step is to study the problem with a numerical model where the data is higher
133 resolution in time and space, and where cause and effect can be more easily isolated. Here we
134 present a calibrated numerical model of Wax Lake Delta built in Delft3D and use it to analyze
135 how sediment retention varies for different flood-wave magnitude, tidal amplitude, and extent of
136 vegetation coverage on the existing deltaic islands. We choose to assess the influence of these
137 three forcing mechanisms because they are continuous in nature, and are the primary drivers of
138 flooding of the deltaic islands. We choose to ignore waves in this study because they are small in
139 the Gulf of Mexico and minimally affect sediment transport around Wax Lake Delta and onto the
140 deltaic islands (Wright & Coleman, 1973,1974). We are interested in how changes in the
141 magnitude of our forcing mechanisms affect sediment retention magnitude and distribution. We
142 calculate the sediment retention for the whole delta and assess the spatial distribution of this
143 retained sediment across subsections (basin, delta front, channels, and islands).

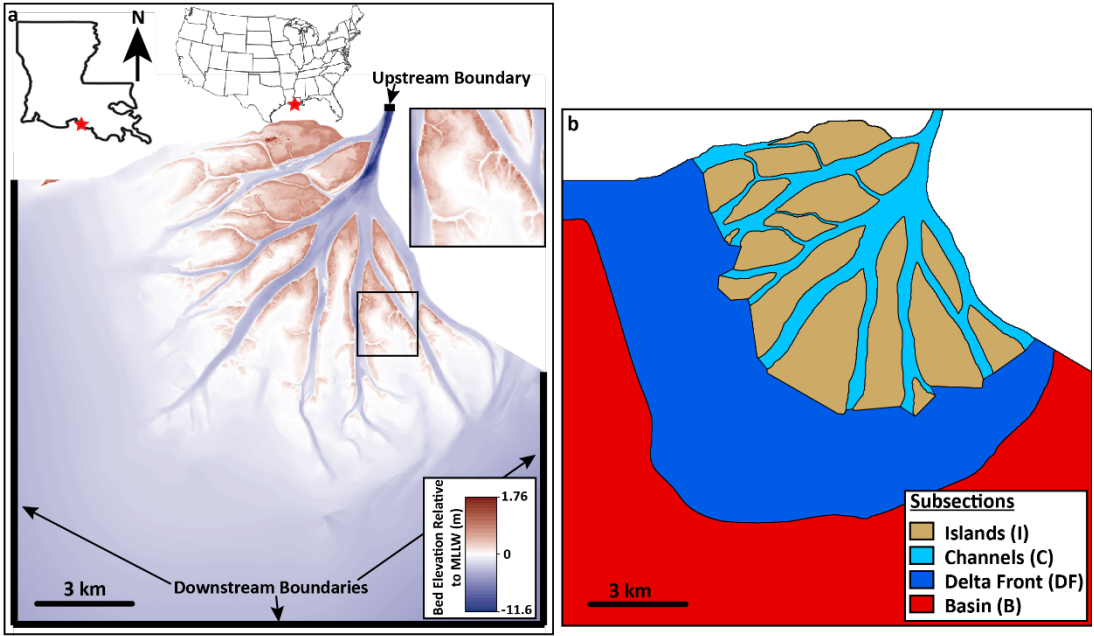
144 **2. Study area**

145 The Wax Lake Delta (WLD) is an actively prograding bayhead delta within the greater
146 MRD system. Located at the mouth of the Wax Lake Outlet (WLO), WLD resulted from
147 anthropogenic diversion of the Atchafalaya River in 1941. First becoming emergent in 1973,
148 WLD experienced rapid growth in the following years due to record flooding in 1973 and 1975
149 (Van Heerden & Roberts, 1988). Upon aggrading to an elevation where overlying water was
150 shallow enough, ruderal plant species have colonized the deltaic islands (Carle et al., 2015).
151 WLD has continued to grow vertically and laterally (Roberts et al., 2003; Kim et al., 2009)
152 Rosen & Xu, 2013; Carle et al., 2015; Olliver & Edmonds, 2017) in a coastal wetland system
153 with some of the highest land-loss rates in the world (Gagliano et al., 1981; Day et al., 2000;
154 Couvillion et al., 2011). While perhaps an unintended product of the Atchafalaya River
155 diversion, WLD serves as an example of what the diversions proposed in Louisiana’s Coastal
156 Protection and Restoration Authority (CPRA) Master Plan hope to accomplish (CPRA, 2017). Its
157 role as a natural field observatory and use as a template in numerical modeling studies can
158 provide insight into how wetlands in these systems develop and what controls sediment retention
159 in them.

160 **3. Methods**

161 **3.1 Modeling domain**

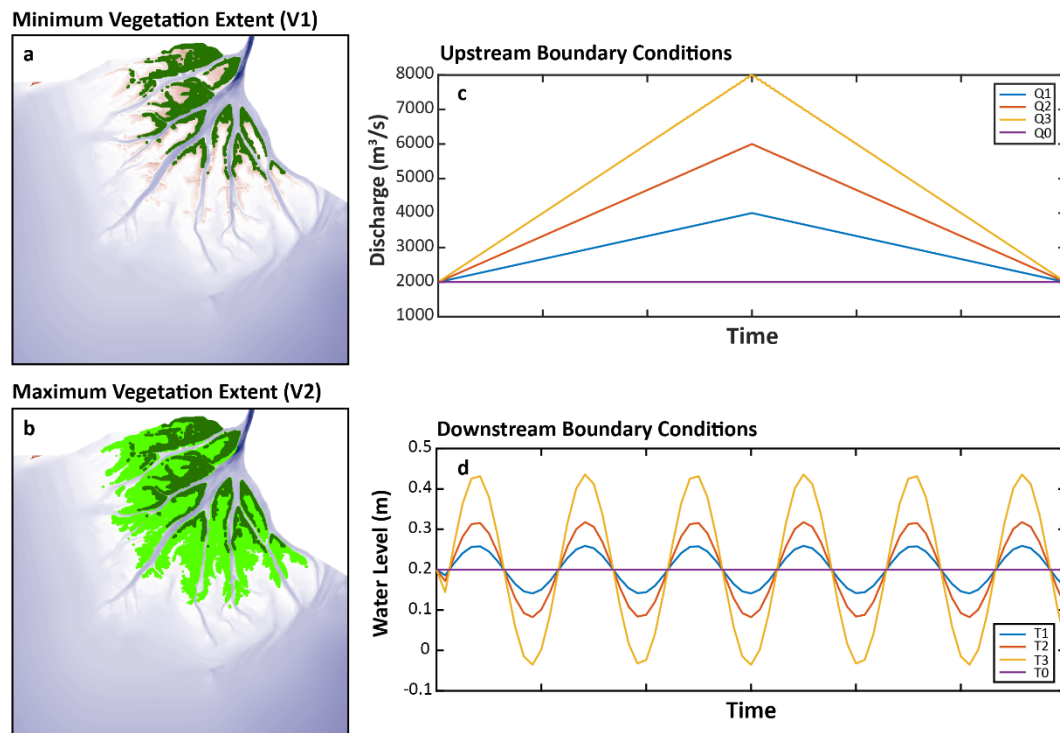
162 To assess the impact of floods, tides, and vegetation on sediment retention within a
163 deltaic system, we constructed a hydrodynamic model of the WLD in Delft3D. Our model of
164 WLD uses a 20 m resolution seamless DEM as the initial bathymetry (Figure 1a). We



165
 166 Figure 1 – (a) Modeling domain and digital elevation model (DEM) of the Wax Lake Delta, LA, USA. The red star
 167 marks the location of our study area in Louisiana. DEM resolution is 20 m x 20 m and the upstream and downstream
 168 model boundaries are marked by bold black lines. The inset image displays how the DEM resolves the primary
 169 features of the delta and also the smaller channels in the island interiors. (b) Subsections of the modeling domain
 170 used for sediment retention and areally-averaged vertical accretion calculations.

171 constructed this DEM using LiDAR data of the subaerial islands collected as part of the USGS
 172 Atchafalaya 2 LiDAR campaign (NOAA, 2015), single beam bathymetry of the delta front
 173 collected in February 2015 and multi-beam bathymetry in the distributary channels collected in
 174 2007, 2009, and 2013 (Shaw et al., 2016; their supplementary material). The 20 m resolution of
 175 our seamless DEM captures the primary channel and island features of the delta, and the smaller
 176 channels within the deltaic islands (Figure 1a, inset). Our modeling domain has an upstream
 177 boundary where we specify the incoming water discharge and suspended sediment and
 178 downstream boundaries where we specify the water level fluctuations due to tides (Figure 1a).
 179 We populate the island tops with vegetation of consistent height (1 m) and stem density (0.25 m^{-2})
 180 ¹), which is calculated assuming ~ 25 stems per square meter and a stem diameter of ~ 1 cm. The
 181 stem diameter is typical of *Typha latifolia* (Kadlec & Wallace, 2008), a common species in WLD
 182 (Johnson et al., 1985). While our spatial density is lower than the ~ 40 stems per square meter

183 typical of *Typha latifolia* (Grace, 1989; Miller & Fujii, 2010), this density is an intermediate
 184 value within the range of stem density considered by Nardin et al., (2016). The interaction
 185 between flow and vegetation is governed by the Baptist (2005) formulation. In this study, we use
 186 two vegetated extent maps, which represent the areal vegetation coverage at minimum and
 187 maximum biomass periods of the year, as well as a no vegetation extent map (Figure 2a,b). The
 188 minimum and maximum vegetated extent maps are based on work presented by Olliver &
 189 Edmonds (2017).



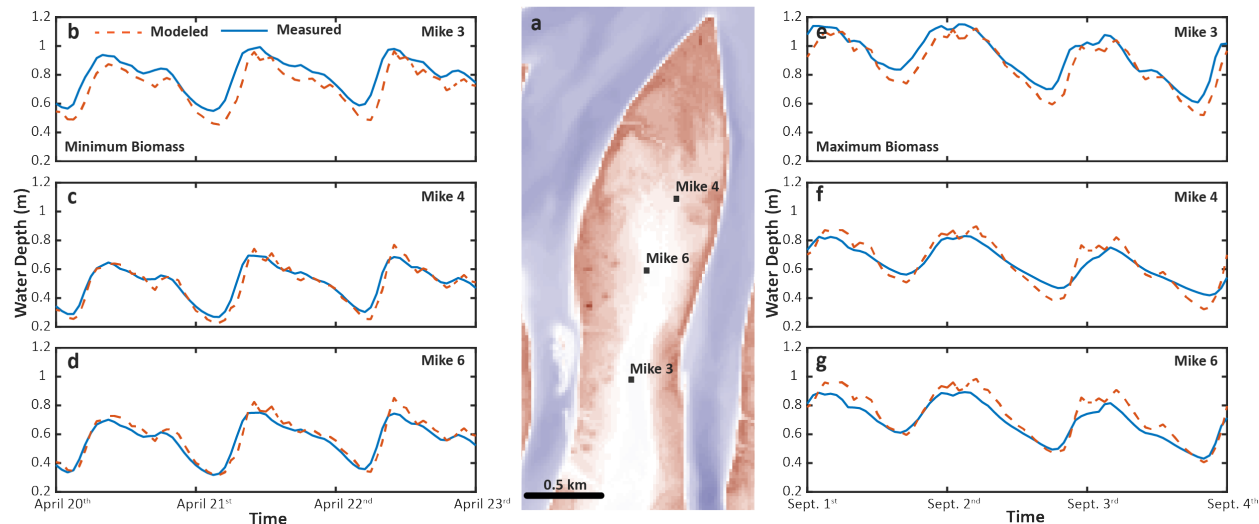
190
 191 Figure 2 – (a-b) The extent of vegetation coverage on the deltaic islands with constant vegetation height (1m) and
 192 density (0.25 m^{-1}) between and throughout for our minimum (V1) and maximum (V2) vegetation extent runs. (c)
 193 The flood waves and (d) tidal amplitudes applied at the upstream and downstream boundary, respectively.

194

195 3.2 Model calibration and validation

196 We calibrated our model using field-collected water depths from several platforms
 197 located in the interior of an island of WLD (Figure 3a). For calibration we used water depths

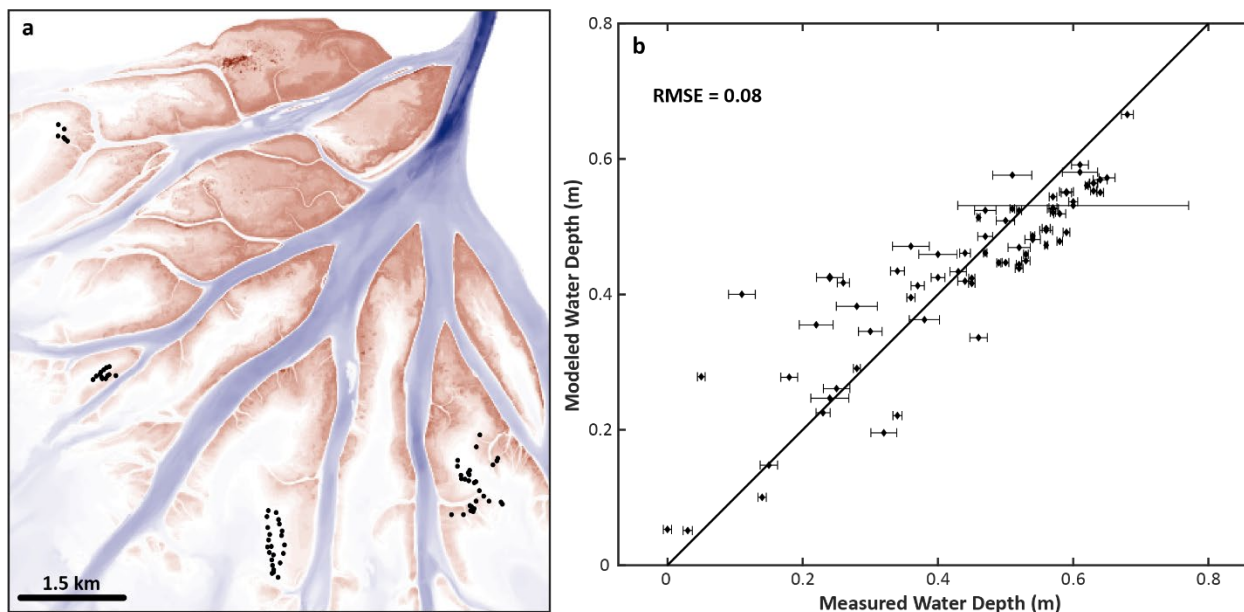
198 from April and September, representing the minimum and maximum biomass, respectively
199 (Figure 2a,b), from three platforms (Figure 3b-g). The calibration model runs were forced with



200
201 Figure 3 – (a) Location of the observation platforms within the interior of Mike Island in WLD. Model calibration
202 results for minimum biomass (b-d) and maximum biomass (e-g) shows good agreement between observed water-
203 depth data observed (solid line) and modeled (dashed line).

204 the water discharge (USGS Calumet gauge on the WLO; Gauge 07381590) and the tidal water
205 levels (NOAA Amerada Pass in the Atchafalaya Delta; Gauge 8764227) over the same time
206 period as the water-depth data was collected. We calibrated the water level in the model to an
207 average root mean square error of 0.06 m between the measured and modeled data (Figure 3b-g).
208 We accomplished this by using different Manning’s roughness of $n = 0.01$ for the channels,
209 unvegetated interdistributary bays, and delta front, and an $n = 0.2$ for areas populated by
210 subaerial vegetation (dark green area, Figure 2a), and an $n = 0.08$ for the vegetated intertidal
211 zone (light green area, Figure 2b). We also had to raise the downstream tidal water levels by 0.2
212 m. This suggests that the gauge in Amerada Pass may not faithfully represent the tidal level in
213 neighboring WLD nearly 15 km away. This is not surprising given that the gauge is located
214 within the channel network of the Atchafalaya Delta, and tidal waves are transformed as they
215 funnel through distributary networks and interact with fluvial discharge (Hoitink & Day, 2016).

216 To validate the model, we compared model output to measured water depths in 72
217 locations that were not used in the calibration. From August 20th to August 23rd, 2014, we
218 collected water depths at discrete points (Olliver & Edmonds, 2017) (Figure 4a). Using the
219 calibrated model, we ran a simulation over the same time period our water-depth data were
220 collected using upstream water discharge from the USGS Calumet gauge and downstream tidal
221 conditions from Amerada Pass with a 0.2 m increase. We then compared the water depth
222 predicted by the model at the exact time we collected the water-depth data in the field. Our
223 calibrated model predicted water depths with a RMSE = 0.08 m as compared to the observed
224 water-depth data across the deltaic islands (Figure 4).



225 Figure 4 – (a) Locations of water depth measurements used for model validation. (b) Measured water depths at
226 locations presented in (a) versus the model-predicted water depths. Solid black line represents a 1:1 fit. Our model
227 accurately predicts water depth to within 8 cm of the observed water depth. The horizontal error bars represent
228 variance of bed elevation within the 20 m cell in which each data point is located as determined using the original 5
229 m resolution seamless DEM.
230

231 3.3 Experimental design and choice of boundary conditions

232 Our modeling is designed to understand how incoming flood-wave magnitude, tidal
233 amplitude, and the extent of island vegetation coverage affects sediment retention. One approach

234 would be to drive the model with measured hydrographs from the Calumet gauge, and tidal
235 fluctuations from Amerada Pass, but that introduces additional variables we are difficult to
236 control for, such as hydrograph shape or tidal irregularities. Instead, we designed the boundary
237 conditions to be generically representative of these processes. This way we could smoothly vary
238 the magnitude of these boundary forcings over parameter space, which allows us to more clearly
239 understand cause and effect.

240 In our model runs the flood-wave magnitude varies over four conditions: a no flood wave
241 condition but constant discharge of $2000 \text{ m}^3\text{s}^{-1}$ ($Q0$), to three different triangular flood waves
242 with a base discharge of $2000 \text{ m}^3\text{s}^{-1}$ and peak discharges of $4000 \text{ m}^3\text{s}^{-1}$ ($Q1$), $6000 \text{ m}^3\text{s}^{-1}$ ($Q2$),
243 and $8000 \text{ m}^3\text{s}^{-1}$ ($Q3$) (Figure 2c). The $Q0$ condition is the average base flow during the spring
244 flood period. Our range of peak discharges are an evenly distributed sampling of low, medium,
245 and high magnitude flood discharges based on the range of discharges observed at the USGS
246 Calumet gauge from 1987 to 2018. We simplify the tidal signal to just the semi-diurnal
247 component and vary over it four conditions: no tide but constant base level of 0.2 m relative to
248 MLLW ($T0$) to three semi-diurnal tides with amplitudes of 0.059 m ($T1$), 0.118 m ($T2$), and
249 0.236 m ($T3$) (Figure 2d). The $T0$ condition is the water-level adjustment to our downstream
250 boundary made during model calibration. The range of tidal amplitudes for conditions $T1$ to $T3$
251 are determined from the range of semi-diurnal components measured at the Amerada Pass gauge,
252 which we center on our baseline of 0.2 m relative to MLLW.

253 The sixteen combinations of discharge and tidal conditions were run for three different
254 vegetation conditions for a total of 48 model runs. Vegetated extent of the islands varies from a
255 null condition of unvegetated ($V0$) to minimum ($V1$) and maximum vegetated extent ($V2$) (Figure
256 2a,b). For $V0$, the alluvial bed roughness is $n = 0.01$ everywhere. For $V1$, the dark green areas

257 (Figure 2a) have $n = 0.2$, and for $V2$, the light green areas have $n = 0.08$ (Figure 2b). All other
258 areas in $V1$ and $V2$ have $n = 0.01$. Vegetation, where present, always has a constant height (1 m)
259 and stem density (0.25 m^{-1}). This choice is clearly a simplification because, although vegetation
260 communities are more complex, we simplified the height and density so that we could focus on
261 how vegetation extent affects sediment retention.

262 We introduce silt ($59 \mu\text{m}$) and freshwater at the upstream boundary over the duration of
263 the model runs. The basin is assumed to contain freshwater throughout the run. The
264 concentration of silt suspended silt is set by an empirically-derived relationship between
265 discharge and suspended sediment concentration from data collected in the WLO by the USGS
266 (Figure A1). We only consider the silt fraction and ignore sand because silt makes up $\sim 91\%$ of
267 the sediment entering WLD (Shaw et al., 2013). In addition, since the system is relatively mature
268 the islands are nourished primarily by silt that is carried higher in the water column, as opposed
269 to the sand that remains in the channels. We set a grain settling velocity of 3 mm s^{-1} . Using
270 Ferguson and Church (2004) this corresponds to an unflocculated grain size of $59 \mu\text{m}$. Based on
271 this settling velocity, we set the critical bed shear stress for sedimentation to 0.01 N m^{-2} . This
272 corresponds to a shear velocity of approximately 3 mm/s , in this way when the bed shear stress is
273 below this value, grain settling exceeds the shear velocity and sedimentation can occur. For
274 simplicity, we eliminate the possibility of erosion or re-suspension of the silt after deposition by
275 setting the critical bed shear stress for erosion at 100 Nm^{-2} , though tests for select model runs
276 indicate this does not change the results. Delf3D calculates suspended load transport by solving
277 the diffusion-advection equation. As we use cohesive sediment in our model, the Partheniades-
278 Krone formulations for erosion and deposition were used (Partheniades, 1965). In Delft3D we
279 set out minimum depth for sediment calculation to 0.1 m . We ran our models for three days

280 model time, with a morphological scale factor of 20 applied so the runs represent 60 days of bed
281 evolution. This 60-day period represents the median duration of a flood pulse down the WLO
282 based on visual inspection of the Calumet gauge discharge records for the winter/spring flood
283 seasons from 1987 to 2018.

284 We assessed how the silt moves through the deltaic system by dividing the modeling
285 domain into four subsections based on hydrological and ecogeomorphic attributes: the
286 distributary channel network (C), deltaic islands (I), delta front (DF), and the basin (B) (Figure
287 1b). The boundary between the channel network and island areas is the wet/dry boundary at the
288 bankfull discharge of $\sim 2000 \text{ m}^3\text{s}^{-1}$. We consider the boundary between each island and the delta
289 front to be the minimally convex hull spanning the two most distal points of vegetated area at
290 maximum biomass. This boundary also roughly coincides with the 0 m relative to MLLW
291 elevation contour. The channel-delta front boundary was defined as a series of minimally convex
292 hulls spanning from the two most distal points of vegetated areas of neighboring islands. Finally,
293 the basin-delta front boundary is set at the -2 m relative to MLLW elevation contour based on
294 work presented by Geleynse et al. (2015).

295 **3.4 Analyses of model runs**

296 For our analyses, we calculate four different quantities that describe retention at different
297 scales. First, we calculate the porosity-adjusted volume of sediment deposited in each subsection
298 ($D_{subsection}, \text{m}^3$) relative to the total incoming silt measured at the upstream boundary (D_o, m^3), a
299 term we refer to as delta-scale retention ($F_{subsection}$) (Equation 1):

$$300 \quad F_{subsection} = \frac{D_{subsection}}{D_o} * 100 \quad (\text{Equation 1})$$

301 Delta-scale, in this sense, refers to the total incoming sediment flux at the upstream
302 boundary and subscript *subsection* refers to one of the four subsections in Figure 1b. Second, for
303 only the islands, we calculate the total incoming silt onto the islands ($D_{o,I}$, m³) relative to D_o , a
304 term we refer to as potential delta-scale retention on the islands ($F_{I,P}$) (Equation 2):

$$305 \quad F_{I,P} = \frac{D_{o,I}}{D_o} * 100 \quad (\text{Equation 2})$$

306 $D_{o,I}$ is calculated by finding the component of the sediment flux vector perpendicular to the
307 boundary of the island for each model grid cell and summing them all. Third, we calculate the
308 total porosity-adjusted volume of sediment deposited on the islands (D_I , m³) relative to $D_{o,I}$,
309 which is the island-scale retention (f_I) (Equation 3):

$$310 \quad f_I = \frac{D_I}{D_{o,I}} * 100 \quad (\text{Equation 3})$$

311 The areally-averaged vertical accretion on the islands resulting from this silt retention was also
312 calculated ($\overline{\Delta d_I}$, cm) (Equation 4):

$$313 \quad \overline{\Delta d_I} = \frac{D_I}{A_I} * 100 \quad (\text{Equation 4})$$

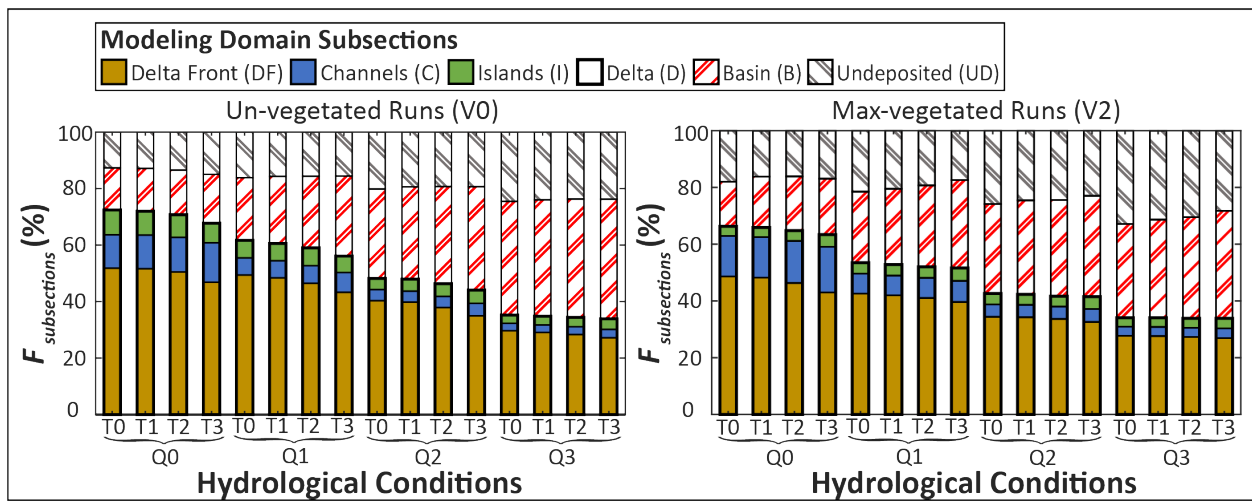
314 where A_I (m²) is the total area of the islands.

315 **4. Results**

316 The results presented here focus on model runs using the *V0* and *V2* vegetated extents
317 (Figure 2a,b). We conducted runs using the *V1* extent, but as we discuss later, these results are
318 nearly identical to *V0* (Table 1). Here we show results illustrating how retention varies at the
319 delta-scale and as a hydrodynamic drivers of river discharge, and tidal amplitude. The effects of
320 vegetation are discussed in the sections of river discharge and tidal amplitude.

321 **4.1 Delta-scale retention**

322 The percentage of silt retained within all the delta subsections ($F_D = F_I + F_C + F_{DF}$) across
 323 our test parameters decreases from 72 to 34% (unvegetated, $V0$) and from 66 to 34% (max-
 324 vegetated, $V2$) with increasing flood-wave magnitude ($Q0$ to $Q3$) (Figure 5). In fact, increasing
 325 Q decreases the proportion of sediment in the topset ($F_I + F_C$) while the proportion retained in
 326 F_{DF} increases (Figure 5, Table 1). This occurs because at higher Q the higher flow velocities



327
 328 Figure 5 – Delta-scale silt retention (F) for each modeling domain subsection for each of our (a) unvegetated ($V0$)
 329 and (b) max-vegetated ($V2$) runs. Along the x-axis, each grouping of four is a flood wave condition ($Q0-3$), with
 330 each bar in a grouping a tidal condition ($T0-3$). On the y-axis, the bars are divided into the proportional amounts of
 331 D_o for each given run retained in each domain subsection. The undeposited subsection represents the proportion of
 332 D_o that has exited the domain or remains in suspension at run conclusion.

333 cause sediment to bypass the delta topset. As a result, silt retention in the basin (F_B) increases
 334 with Q from 15 to 42% ($V0$) and 16 to 38% ($V2$). The proportion of D_o that exits the domain at
 335 the downstream boundary or remains in suspension when the run ends (F_{UD}) also increases from
 336 13 to 24% ($V0$) and 18 to 28% ($V2$) with increasing Q (Figure 5, Table 1).

337 An increase in tidal amplitude ($T0$ to $T3$) reduces delta-scale retention, F_D , by 3 to 5% at
 338 $Q0$, but by only $\sim 1.5\%$ at $Q3$ (Figure 5, Table 1). Most of this reduction is accommodated by

339 decreasing F_{DF} with increasing Q . But interestingly, F_C and F_I have a more variable response and
340 show increases or decreases with increasing Q at different vegetative conditions (Table 1).

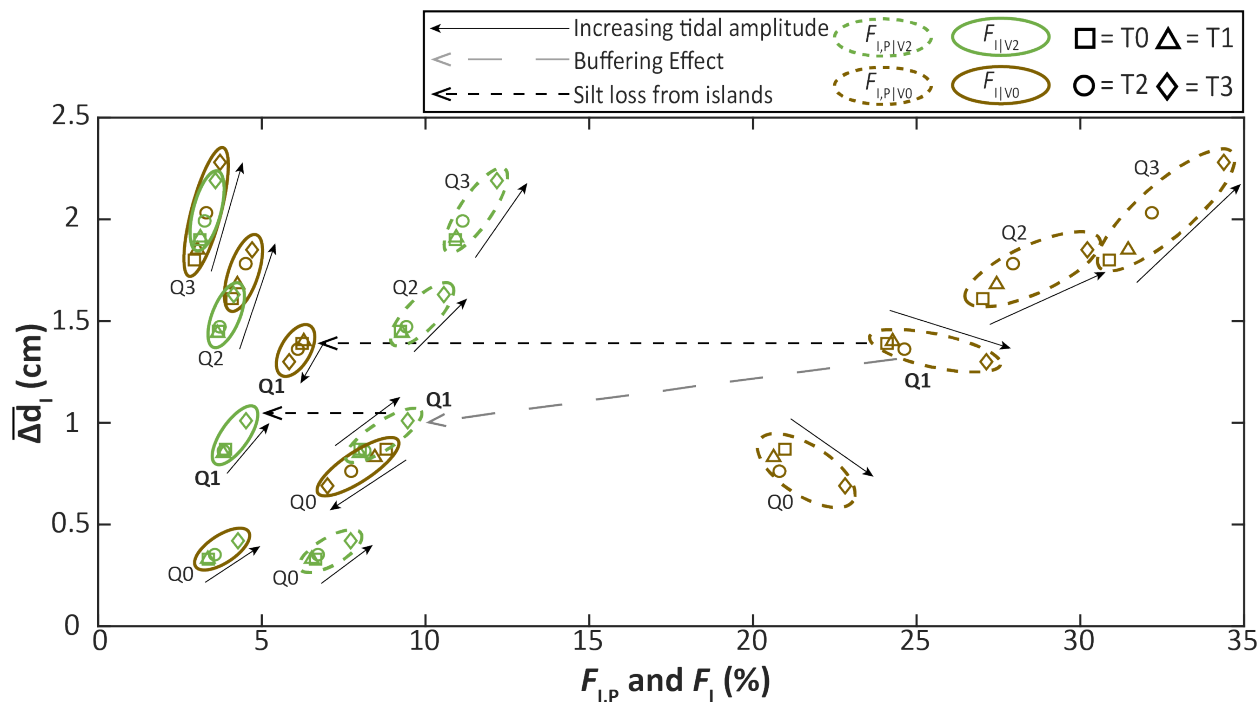
341 The presence of vegetation reduces F_D from $\sim 6\%$ at $Q0$ to $\sim 0.5\%$ at $Q3$ (Figure 5, Table
342 1). Specifically, from $V0$ to $V2$ retention in the delta front (DF) and islands (I) decreases by 1 to
343 4% and 0.5 to 5%, respectively, while retention in the channels (C) increases by 0.5 to 3%.
344 Conversely, vegetation increases retention in the basin (B) from 1 to 5%, as well as the
345 proportion of D_o that remains undeposited (from 2 to 8%). However, regardless of flood-wave
346 magnitude, tidal amplitude, or vegetation, the majority of sediment retained within the delta is
347 deposited in the delta front (52 to 27%), followed by the channels (14 to 3%) and islands (8 to
348 3%) (Figure 5; Table 1).

349 Surprisingly, there is almost no difference in retention for the $V0$ and $V1$ condition across
350 our runs (Table 1). This suggests to us that, as least for the range of parameters considered in this
351 study, the minimal vegetation condition behaves like a completely unvegetated delta.

352 **4.2 The role of flood-wave magnitude**

353 The amount of sediment that flows onto the deltaic islands is an interesting quantity since
354 deltaic islands make up the subaerial landscape, and to keep pace with relative sea-level rise they
355 must be nourished by sediment. $F_{I,P}$ is the proportion of sediment that flows onto the islands and
356 we call it the potential retention because it is the maximum amount of sediment that could be
357 deposited. The difference between the potential retention for the $V0$ and the $V2$ conditions
358 $(F_{I,P}|_{V0} - F_{I,P}|_{V2})$ is a quantity we term as the vegetation buffering effect (Figure 6; length of
359 dashed grey arrow denotes magnitude of buffering effect). For a given vegetation condition, the
360 difference between incoming sediment and deposited sediment $(F_{I,P} - F_I)$ is the percentage of silt

361 (relative to D_0) is not deposited, something we term silt loss (Figure 6; length of dashed black
 362 arrow denotes magnitude of silt loss). The $F_{I,P}$ and F_I results cluster according to flood-wave
 363 magnitude and vegetated extent, and each cluster contains four points that correspond to different
 364 tidal amplitudes (Figure 6; $F_{I,P}$ and F_I clusters outlined by dashed and solid lines, respectively).



365
 366 Figure 6 – The relationship between sediment retention and accretion at the delta-scale. The data clusters are labeled
 367 by flood wave conditions ($Q0-3$) and outlined by dashed and solid lines for the $F_{I,P}$ and F_I data, respectively. The
 368 brown or green color of the cluster outlines denotes the $V0$ and $V2$ condition, respectively. The dashed grey arrow
 369 denotes the buffering effect, whereas the dashed black arrows denote the loss of silt from the islands. Similar lines
 370 could be drawn along all runs but are omitted for clarity. The solid black arrows alongside each $F_{I,P}$ and F_I grouping
 371 highlights the trend of increasing tidal amplitude.

372 The magnitude of the buffering effect ($F_{I,P}|_{V0} - F_{I,P}|_{V2}$) changes as a function of
 373 discharge. As Q increases, so do $F_{I,P}$ and $\overline{\Delta d}_I$ for both the $V0$ and $V2$ runs because larger floods
 374 transport more sediment onto the islands. However, the $V2$ runs have lower $\overline{\Delta d}_I$, and much lower
 375 $F_{I,P}$, compared to $V0$. Thus, at $Q0$ the buffering effect reduces $F_{I,P}$ by roughly 14%, whereas at
 376 $Q3$ the buffering effect reduces $F_{I,P}$ by about 20% (Figure 6, Table 2). If we view the buffering

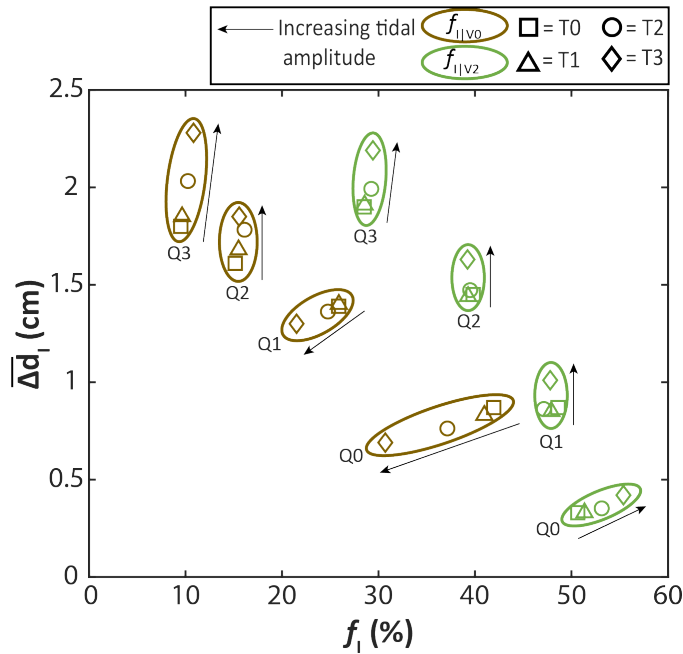
377 effect proportionally then $\frac{Q_{s,I}|_{V2}}{Q_{s,I}|_{V0}} \approx 67\%$ for nearly all runs. The consistency of this proportion is
378 likely because we do not vary vegetation parameters, such as height and density, among our runs.

379 As Q increases, the percentage of sediment deposited in the islands, F_I , decreases, while
380 $\overline{\Delta d_I}$ increases (Figure 6). This is especially true for the $V0$ condition. This negative trend is
381 opposite of the positive trend for $F_{I,P}$ and this arises because silt loss increases with higher Q
382 (Figure 6; dashed black arrow). Even though $F_{I,P}$ increases at higher Q , there is less retention on
383 the islands because increased water depths and velocities across the islands advect more
384 sediment off them. The data for $V2$ show similar behavior, but the silt loss ($F_{I,P}|_{V2} - F_I|_{V2}$) at a
385 given Q is not as great as $V0$ because vegetation increases sediment retention by decreasing
386 sediment advection off the islands.

387 The tendency of vegetation to increase sediment retention is something we term the
388 trapping effect. Though we do not directly measure the trapping effect, it is the complementary
389 percentage with silt loss (dashed black arrow, Figure 6, Table 2). For both $V0$ and $V2$, the
390 quantity $F_{I,P} - F_I$ increases with Q . But importantly, both the magnitude of silt loss and the
391 increase in silt loss with increasing Q is much greater for the $V0$ condition than for the $V2$
392 condition (Figure 6; Table 2). The consistently smaller decrease from $F_{I,P}$ to F_I for the $V2$
393 condition shows how vegetation contributes to silt retention.

394 To consider the trapping effect more directly, we shift our perspective and consider
395 island-scale retention (f_I), which is sediment deposition relative to the sediment flux onto the
396 islands ($D_{o,I}$) rather than relative to the total sediment entering the deltaic system at the upstream
397 boundary (D_o). From this perspective, vegetation increases retention (~ 28 to 55%) compared to
398 the unvegetated condition (~ 9 to 42%) for a given flood-wave magnitude and tidal amplitude

399 (Figure 7). f_i decreases with greater flood-wave magnitude for $V0$ and $V2$, which underscores that
 400 while vegetation enhances silt retention on the islands, this trapping effect becomes less effective
 401 at higher Q .



402
 403 Figure 7 – The relationship between sediment retention and accretion at the island-scale. The data groupings are
 404 labeled by flood-wave conditions ($Q0-3$) and outlined by solid brown and green lines denoting the $V0$ and $V2$ runs,
 405 respectively. The solid black arrow alongside each f_i grouping highlights the trend of increasing tidal amplitude.

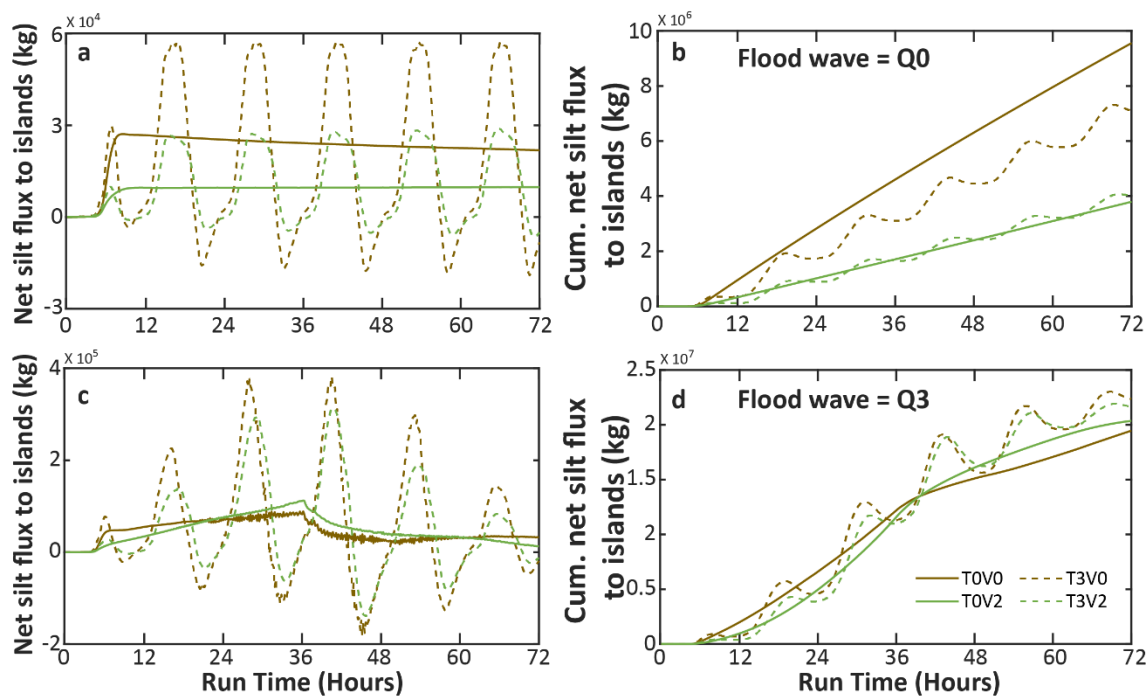
406 4.3 The role of tidal amplitude

407 As already discussed, each Q and vegetation condition cluster contains four points that
 408 correspond to different tidal amplitudes (Figures 6 and 7). Tidal amplitude has a smaller
 409 influence on silt retention over the entire delta (Figure 5) and within the deltaic islands (Figures 6
 410 and 7), compared to flood-wave magnitude or the presence of vegetation. But, the effect of tidal
 411 amplitude is not monotonic; in some cases tides increase retention and in other cases they
 412 decrease it.

413 Regardless of vegetation or flood-wave magnitude, tides increase $F_{I,P}$ by roughly 1 to 3%
 414 for $V0$ and $V2$ conditions (Figure 6). This occurs because greater tidal amplitude increases island

415 inundation and transports more silt onto the islands. However, as tides recede, they also transport
 416 suspended silt out of the islands and this effect can offset the increase in $F_{I,P}$. Notice that for
 417 most of our runs, greater tidal amplitude results in greater F_I or f_I (Figures 6 and 7). However, for
 418 the $V0$ condition at $Q0$ and $Q1$ the opposite is true, and lower tidal amplitude results in greater
 419 silt retention (Figures 6 and 7). This reversal never occurs for the $V2$ condition.

420 This reversal does not occur for $V2$ because the trapping effect of vegetation limits
 421 sediment export from the islands as the tide recedes. To see this, we plot the instantaneous and
 422 cumulative net silt flux from each model timestep (Figure 8). We define net silt flux as the total
 423 silt flux into the islands minus the amount that fluxes out of the islands. At $Q0$ runs with tides in



424
 425 Figure 8 – (a,c) Instantaneous net silt flux to all islands over the course of the runs for the null ($T0$, solid) and max
 426 tidal amplitude ($T3$, dashed) and for the null ($Q0$) and max flood wave ($Q3$). (b,d) Cumulative net silt flux over the
 427 course of the aforementioned runs. Both the unvegetated ($V0$, brown) and vegetated ($V2$, green) conditions for these
 428 flood wave and tidal amplitude end member runs are presented.

429 the absence of vegetation ($T3V0$) result in higher instantaneous net flux compared to the no tide
 430 condition ($T0V0$), but also result in periods of negative instantaneous net flux when more silt

431 leaves the islands than enters (Figure 8a). When no tide is present ($T0V0$, $T0V2$), the
432 instantaneous net silt flux remains at a lower but consistently positive value. The cumulative net
433 silt flux shows that the increased flux during high tide does not offset the sediment exported
434 during low tide, and the result is that tides lower the cumulative flux at $Q0$ and $V0$ conditions
435 (Figure 8b; dashed brown line is below solid brown line). But for the $V2$ conditions, the trapping
436 effect of vegetation reduces silt loss from the islands and the benefit of tides outweighs the
437 detriment, creating a small increase in cumulative net flux (Figure 8a,b; dashed green line is
438 slightly above the solid green).

439 At $Q3$ however, the enhanced silt delivery to the islands offsets the loss caused by tides,
440 even in the absence of vegetation. The $V0$ and $V2$ condition show similar values of net
441 instantaneous flux at high and low tide (Figure 8d). Initially, the cumulative fluxes for all
442 conditions are also similar, but by 60 hours of model runtime the cumulative flux for runs with
443 tides becomes larger than without tides, indicating the net benefit of tides at higher Q (Figure 8d;
444 dashed brown and green lines are higher than corresponding solid lines at the end of the run).

445 **5. Discussion**

446 **5.1 How the competing effects of buffering and trapping govern the vegetation** 447 **sedimentation feedback**

448 One of the prevailing notions in ecogeomorphology is that, all else being equal, the
449 presence of above-ground vegetation on the marsh surface can enhance sediment deposition by
450 reducing turbulence and flow velocities in the water column, which promotes the settling of
451 sediment out of suspension (Leonard & Luther, 1995; Christiansen et al., 2000; Morris et al.,
452 2002; Neumeier & Ciavola, 2004; Kirwan & Murray, 2007; Fagherazzi et al., 2012). This

453 enhanced sedimentation does not always occur because sparse vegetation can increase turbulence
454 and limit deposition (Larsen, 2019). Vegetation also reduces bed shear stress thereby limiting
455 remobilization of sediment following initial deposition (Christiansen et al., 2000; Howes et al.,
456 2010). The tendency of vegetation to enhance sedimentation is often formalized as a positive
457 feedback (Larsen, 2019), especially in models of salt marshes (Kirwan & Murray, 2007;
458 Fagherazzi et al., 2012 and references therein) and fluvial floodplains (Kleinhans et al., 2018 and
459 references therein), where the presence of vegetation, up to a point, causes faster rates of vertical
460 surface accretion. This positive vegetation-sedimentation feedback in our study is manifested as
461 the sediment trapping effect. Another well-documented effect of vegetation is the occurrence of a
462 stress-divergence feedback. As water interacts with an isolated patch of vegetation, the
463 difference of roughness between the vegetation and the smoother bed surrounding it causes stress
464 to diverge and concentrates flow along the patch margins where there is less resistance
465 (Weerman et al., 2010; Temmerman et al., 2005, 2007; Nardin & Edmonds, 2014; Nardin et al.,
466 2016; Larsen, 2019; Yamasaki et al., 2019 and references there in). This can lead to erosion at
467 the patch margin, further concentration of flow, and eventual channelization. While we did not
468 simulate planform development and channelization in our model, this stress-divergence feedback
469 is the mechanism in our runs that creates the buffering effect, which reduces sediment transport
470 onto the islands due to the presence of vegetation (Weerman et al., 2010).

471 The trapping and buffering effects together determine whether vegetation causes an
472 increase or decrease in sedimentation in a morphodynamic system. An interesting result of our
473 modeling experiments is that in all scenarios tested here, vegetation is ultimately a negative
474 feedback and results in less sedimentation ($V2$ clusters always have equal or less $\overline{\Delta d}_I$ than $V0$
475 clusters, Figures 6 and 7). This stands in contrast to previous studies where vegetation causes an

476 increase in sedimentation compared to unvegetated conditions (Kirwan & Murray, 2007;
 477 Fagherazzi et al., 2012; Larsen, 2019). This arises in our results because the buffering effect is
 478 always larger than the trapping effect for our chosen vegetation height and density conditions.
 479 The buffering and trapping effects can be tracked on Figure 6 by following the trajectory from
 480 $F_{I,P}|_{V0} \rightarrow F_{I,P}|_{V2} \rightarrow F_I|_{V2}$ for any given discharge condition. For example, at $Q1$ $F_{I,P}|_{V2}$ is less
 481 than $F_{I,P}|_{V0}$ because of the buffering effect (Figure 6, dashed grey arrow). The amount retained
 482 on the islands, $F_I|_{V2}$, is lower than the incoming flux $F_{I,P}|_{V2}$ (Figure 6, dashed black arrows)
 483 because some silt is lost from the islands. For $Q0$, $Q1$, $Q2$ the combined effects of buffering
 484 ($F_{I,P}|_{V0} \rightarrow F_{I,P}|_{V2}$ dashed gray line) and silt loss from the islands ($F_{I,P}|_{V2} \rightarrow F_I|_{V2}$ dashed black
 485 arrow) are always larger than the silt loss for unvegetated conditions ($F_{I,P}|_{V0} \rightarrow F_I|_{V0}$ dashed
 486 black arrow Figure 6). Because of this, the $V2$ conditions have smaller F_I and $\overline{\Delta d}_I$ than $V0$
 487 conditions.

488 Consistent with general expectations for vegetated surfaces, at $Q1$ the silt loss from the
 489 islands ($F_{I,P} \rightarrow F_I$) is greater for $V0$ than $V2$ because vegetation enhances sediment trapping.
 490 Interestingly, at $Q3$ for both $V0$ and $V2$, F_I and $\overline{\Delta d}_I$ are nearly identical. This suggests that at high
 491 discharge the trapping effect balances out the buffering effect. A reasonable conjecture would
 492 then be that at discharges higher than $Q3$ vegetation might result in higher retention and more
 493 deposition. While this is sensible, the peak discharge for the $Q3$ condition we model here (8000
 494 $\text{m}^3 \text{s}^{-1}$) is nearly the maximum observed discharge at Wax Lake Outlet and does not recur often.
 495 Because of this, it seems unlikely that under reasonable hydrologic conditions vegetation will
 496 create higher sedimentation on WLD. However, we only used one set of vegetation
 497 characteristics in our runs and the interaction of the buffering and trapping effects may vary in

498 relation to these characteristics (Nardin & Edmonds, 2014; Nardin et al., 2016). In addition, there
499 are vegetation effects we do not simulate, such as direct capture (Strumpf, 1983; Yang et al.,
500 2008; Larsen, 2019), which we assume is small compared to direct deposition.

501 Our model results imply the vegetation only enhances deposition over unvegetated
502 conditions if the trapping effect overcomes the buffering effect. This balancing act between
503 trapping and buffering is not usually considered or parameterized in models. This could be, in
504 part, because many studies on vegetation and sedimentation focus on salt marsh environments
505 (e.g., Fagherazzi et al., 2012 and references therein) where the buffering effect is minimized
506 because sediment and water flow into a closed tidal basin. In closed tidal basins, water and
507 sediment enter and exit through the same cross-section, and the presence of vegetation
508 predominately affects the location along the tidal channel network that sediment enters the
509 marsh, but not the total sediment flux onto the marsh surface (Temmerman et al., 2005, 2007). In
510 deltaic marshes, on the other hand, the basin is not closed, and water and sediment can flow onto
511 the marshes, or bypass them completely by flowing through the channel network and into the
512 ocean.

513 Because deltas are not closed basins, an important next step is to map out the conditions
514 where the trapping and buffering effects lead to enhanced or decreased sedimentation. In the runs
515 we only used one set of vegetation characteristics, but previous work on a generic delta suggests
516 that there may be optimal vegetation height and density where the trapping effect is greater than
517 the buffering effect (Nardin & Edmonds, 2014; Nardin et al., 2016). Future work could try to
518 map out buffering and trapping effects relative to one another and define when vegetation-
519 sedimentation feedback in deltaic marshes is positive or negative. An important point to make,
520 however, is that our experiments did not allow for erosion of the substrate or resuspension of

521 sediment following initial deposition. This effectively maximizes the trapping effect, and if this
522 limitation is relaxed then vegetation may produce an even more drastic decrease in
523 sedimentation.

524 **5.2 Operational considerations and trade-offs for sediment diversions**

525 Efforts towards mitigation and reversal of wetland loss in coastal deltaic wetlands, like
526 the MRD, often consider vertical accretion as a measure of success. Because vertical accretion is
527 so important, inorganic sediment is one of the most valuable resources along disappearing
528 coastlines. But, river management structures, like dams and levees, have reduced sediment
529 supply to the coast making it important to achieve vertical accretion of the marsh platform with
530 efficient sediment retention. As one might guess, in river-dominated deltas like the one studied
531 here, big floods lead to significant sediment deposition in the delta and on the islands (Snedden
532 et al., 2007; Kolker et al., 2012; Esposito et al., 2013; Rosenheim et al., 2013; Carle et al., 2015;
533 Shen et al., 2015; Bevington et al., 2017). But, that comes at a tradeoff because as vertical
534 accretion goes up, sediment retention goes down (Figures 6 and 7). Fieldwork by Keogh et al.
535 (2019) showed similar results. Thus, while larger flood waves may enhance vertical accretion of
536 existing wetlands (a desired outcome of sediment diversion construction), it comes at the cost of
537 lower sediment retention in the delta.

538 Based on the fieldwork in the Davis Pond diversion, Keogh et al. (2019) proposed a
539 conceptual model that suggests an optimal discharge range for sediment deposition, beyond
540 which deposition will decrease. Our deposition results for the deltaic islands do not follow this
541 conceptual model because deposition increases monotonically up to the highest magnitude flood
542 wave WLD is likely to experience. The inconsistency between our results and the Keogh et al.
543 (2019) conceptual model may be due to the differences in the scales of sediment retention

544 discussed. Our results focus on deposition within the deltaic islands, while Keogh et al. (2019)
545 considers deposition within the entire David Pond basin. Additionally, Keogh et al. (2019)
546 developed the conceptual model based on data extrapolated from limited data (average
547 discharges for winter/spring and summer/fall for one year), which lie on the lower end of the
548 discharge range for the diversion. Thus, our results indicate for the WLD system higher rather
549 than intermediate discharges should be considered for diversion operations if the goal is to
550 maintain or aggrade existing wetlands.

551 Timing of operations is another important factor to consider when seeking to maximize
552 land-building potential of a sediment diversion. Peyronnin et al. (2017) suggested operational
553 strategies for the Mid-Barataria Sediment Diversion by identifying periods of the annual
554 hydrograph during which diversion operations would maximize land building while seeking to
555 limit detrimental impact to the existing ecosystem. Focusing diversion operations in the winter
556 and/or early spring to take advantage of the higher concentration of sand, silt, and clay typically
557 carried by the first peak of the water year (Peyronnin et al., 2017; Allison et al., 2012).
558 Operations later in the year should seek to operate the diversion on the rising limb of flood peaks
559 in order in order to capture as much sediment in the diversion as possible, per unit of freshwater
560 entering the diversion (Peyronnin et al., 2017). Additionally, Peyronnin et al. (2017) suggested
561 winter operation while vegetation is senesced could reduce vegetation stress and loss from
562 prolonged flooding. Our study further supports that operations be focused in the winter/early
563 spring period of the year, because during this period of the year larger magnitude discharges
564 occur and vegetation is senesced; both conditions create greater vertical accretion of existing
565 wetlands (Figures 6 and 7). However, it should be kept in mind, as stated earlier, maximizing this
566 vertical accretion will come at the cost of sediment retention due to greater throughput to the

567 basin. While more work is required on the subject, we note the suggestion by Peyronnin et al.
568 (2017) that cold fronts during the winter/spring could help maximize sediment resuspension and
569 transfer back onto wetland surface from the basin, which could help improve sediment retention
570 and further improve vertical accretion.

571 Finally, while perhaps the smallest influence considered in our study, our results show
572 tides have an important impact on sediment retention and deposition, even in the face of high
573 discharges (Figures 6 and 7). Consider that at $Q3$ for the $V0$ condition, the $T3$ amplitude results
574 in a ~ 0.5 cm increase in $\overline{\Delta d}_I$ compared to $T1$. Thus at higher Q , tides enhance deposition with
575 minimal change to retention (Figures 6 and 7). In this way, if diversion operations are timed with
576 higher spring tides it could create more vertical accretion. Furthermore, larger tidal amplitudes
577 also may help mitigate sediment loss from the deltaic system by reducing higher flood velocities
578 that move sediment into the basin (Wright, 1977). F_{DF} decreases with greater tidal amplitude,
579 suggesting this reducing effect fails to retain more sediment on the distal edge of the delta (Table
580 1). However, F_B increases, while F_{UD} decreases with greater tidal amplitude, indicating greater
581 tidal amplitudes may be helping to retain more sediment in the basin adjacent to the delta and
582 possibly contribute to reduced transport of sediment offshore (Table 1). Finer spatial analyses of
583 where within the basin this retained sediment is deposited would help clarify this. It should also
584 be noted our delineation of the delta front/basin boundary was only one of various possible
585 definitions. A different boundary definition may place the boundary further seaward, resulting in
586 different F_{DF} and F_B trends, and thus points to the need for standardization and wide application
587 of the definition for the delta front/basin boundary in future studies.

588 **6. Conclusion**

589 In this study we used a calibrated numerical model of the Wax Lake Delta (WLD) to
590 consider how river discharge, tidal amplitude, and vegetation extent influence sediment
591 retention. The most important factor for sediment retention is river discharge because that is the
592 primary supplier of sediment. As discharge increases, vertical accretion of existing wetlands
593 increases, but sediment retention, relative to the total incoming flux, across the whole delta
594 decreases from 72 to 34% because more sediment bypasses the delta to the basin. This highlights
595 an important tradeoff for sediment-starved deltas: enhanced deposition comes at the expense of
596 lower retention.

597 We find that in all scenarios tested here vegetation is ultimately a negative feedback and
598 results in less vertical accretion of the islands and lower sediment retention than if vegetation is
599 not present or senesced. This occurs because of the interaction of the buffering and trapping
600 effects of vegetation. Buffering reduces sediment flux onto islands, whereas trapping enhances
601 deposition, and in our run the buffering effect is always greater than trapping. But, we only
602 modeled one vegetation condition and more study is needed to consider how variations in
603 vegetation height and/or density alter this outcome.

604 Larger tidal amplitudes increase vertical accretion at higher discharges and they may help
605 to reduce sediment bypass to the basin. Thus, our findings indicate timing of diversion operations
606 during higher amplitude tides, in the winter/spring months when discharges are typically higher
607 in the MRD system and vegetation is senesced may be best for maximizing vertical accretion of
608 existing wetlands.

609
610
611

612 Table 1 – Delta-scale silt retention ($F_{subsection}$) for $V0$, $V1$, and $V2$ conditions. $V0$ and $V2$ data are shown in Figure 5. D = delta (DF + C +I), DF = delta front, C =
613 delta channels, I = delta islands, B = basin, and UD = undeposited. See Figure 1b for the locations of domains, DF, C, I, and B.

	$F_{DF V0}$	$F_{DF V1}$	$F_{DF V2}$	$F_C V0$	$F_C V1$	$F_C V2$	$F_I V0$	$F_I V1$	$F_I V2$	$F_D V0$	$F_D V1$	$F_D V2$	$F_B V0$	$F_B V1$	$F_B V2$	$F_{UD} V0$	$F_{UD} V1$	$F_{UD} V2$
Q0T0	51.82	49.30	48.67	11.82	14.56	14.26	8.80	8.44	3.36	72.44	72.30	66.29	14.90	15.01	15.66	12.66	12.69	18.05
Q0T1	51.63	49.09	48.19	11.91	14.68	14.36	8.45	8.09	3.35	71.99	71.85	65.91	15.13	15.34	17.95	12.87	12.81	16.14
Q0T2	50.47	48.01	46.34	12.27	15.11	14.81	7.74	7.44	3.58	70.48	70.55	64.73	16.03	15.99	19.15	13.49	13.46	16.12
Q0T3	46.84	44.42	42.98	14.01	16.95	16.07	7.01	6.65	4.27	67.85	68.01	63.32	17.19	17.04	19.78	14.96	14.94	16.90
Q1T0	49.40	48.92	42.56	6.07	6.83	7.05	6.23	6.19	3.89	61.70	61.94	53.50	22.14	21.47	25.03	16.16	16.59	21.47
Q1T1	48.40	47.90	42.00	6.05	6.76	6.98	6.28	6.24	3.83	60.73	60.90	52.81	23.58	23.03	26.69	15.69	16.07	20.51
Q1T2	46.48	46.01	41.07	6.24	6.89	7.09	6.11	6.03	3.85	58.84	58.93	52.01	25.55	25.23	28.69	15.61	15.84	19.30
Q1T3	43.30	42.96	39.64	6.97	7.46	7.44	5.84	5.74	4.52	56.10	56.16	51.60	28.37	28.13	30.96	15.53	15.71	17.43
Q2T0	40.34	40.28	34.44	3.94	4.03	4.34	4.09	4.07	3.68	48.38	48.37	42.46	31.48	31.61	31.66	20.14	20.02	25.88
Q2T1	39.81	39.75	34.31	3.91	3.97	4.34	4.25	4.21	3.65	47.97	47.93	42.29	32.62	32.62	33.14	19.41	19.46	24.56
Q2T2	37.88	37.83	33.68	3.98	4.07	4.39	4.52	4.49	3.73	46.38	46.39	41.80	34.35	34.14	33.77	19.27	19.47	24.43
Q2T3	34.96	35.03	32.62	4.39	4.41	4.59	4.70	4.64	4.14	44.05	44.08	41.35	36.61	36.36	35.68	19.34	19.56	22.97
Q3T0	29.65	29.67	27.75	2.66	2.65	3.23	2.94	2.84	3.11	35.24	35.16	34.09	40.24	40.34	33.00	24.52	24.50	32.91
Q3T1	29.06	29.11	27.63	2.68	2.64	3.24	3.04	2.94	3.12	34.78	34.69	34.00	41.27	41.43	34.66	23.95	23.87	31.34
Q3T2	28.38	28.40	27.30	2.71	2.68	3.29	3.32	3.22	3.27	34.41	34.30	33.85	41.87	41.87	35.67	23.73	23.83	30.48
Q3T3	27.21	27.30	26.92	2.96	2.87	3.40	3.72	3.65	3.58	33.89	33.81	33.90	42.34	42.20	37.84	23.77	23.99	28.25

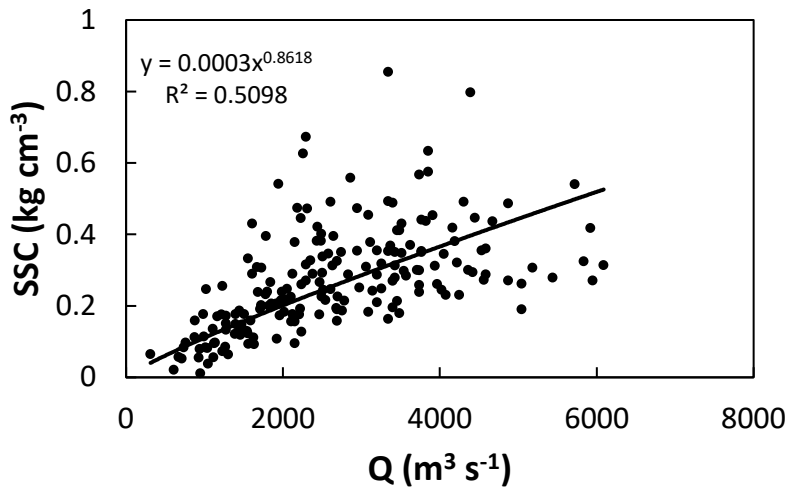
614
615
616
617
618
619
620
621

622 Table 2 – Average vertical accretion, and delta-scale (F) and island-scale (f) sediment retention for the $V0$ and $V2$ conditions. These data are plotted in Figures 6
 623 and 7.

	$F_{L,P V0}$	$F_{L,P V2}$	Buffering effect $F_{L,P V0} - F_{L,P V2}$	$F_I V0$	$F_I V2$	Trapping Effect $F_{L,P V0} - F_I V0$	Trapping Effect $F_{L,P V2} - F_I V2$	$f_I V0$	$f_I V2$	$\overline{\Delta d}_I V0$	$\overline{\Delta d}_I V2$
<i>Q0T0</i>	20.98	6.64	14.33	8.80	3.36	12.18	3.28	41.95	50.65	0.87	0.33
<i>Q0T1</i>	20.63	6.52	14.11	8.45	3.35	12.18	3.17	40.97	51.35	0.83	0.33
<i>Q0T2</i>	20.82	6.73	14.09	7.74	3.58	13.08	3.15	37.19	53.18	0.76	0.35
<i>Q0T3</i>	22.81	7.72	15.10	7.01	4.27	15.80	3.45	30.70	55.38	0.69	0.42
<i>Q1T0</i>	24.09	8.00	16.09	6.23	3.89	17.86	4.11	25.87	48.60	1.39	0.87
<i>Q1T1</i>	24.27	7.99	16.28	6.28	3.83	17.99	4.16	25.89	47.90	1.40	0.85
<i>Q1T2</i>	24.64	8.15	16.48	6.11	3.85	18.53	4.30	24.81	47.18	1.36	0.86
<i>Q1T3</i>	27.13	9.45	17.67	5.84	4.52	21.29	4.93	21.51	47.79	1.30	1.01
<i>Q2T0</i>	27.02	9.24	17.79	4.09	3.68	22.93	5.56	15.15	39.81	1.61	1.45
<i>Q2T1</i>	27.44	9.28	18.16	4.25	3.65	23.19	5.63	15.50	39.28	1.68	1.44
<i>Q2T2</i>	27.95	9.43	18.53	4.52	3.73	23.43	5.70	16.17	39.55	1.78	1.47
<i>Q2T3</i>	30.21	10.56	19.65	4.70	4.14	25.51	6.42	15.57	39.22	1.85	1.63
<i>Q3T0</i>	30.88	10.91	19.98	2.94	3.11	27.94	7.80	9.52	28.51	1.80	1.90
<i>Q3T1</i>	31.46	10.94	20.52	3.04	3.12	28.42	7.82	9.65	28.56	1.85	1.91
<i>Q3T2</i>	32.20	11.15	21.05	3.32	3.27	28.88	7.88	10.30	29.30	2.03	1.99
<i>Q3T3</i>	34.38	12.18	22.20	3.72	3.58	30.66	8.60	10.83	29.42	2.28	2.19

624

625 **Supplemental Figure**



626

627 Figure A1 – Measured water discharge and suspended sediment concentration observed at the USGS Calumet gauge
628 (Gauge 07381590) in the WLO. We use the empirically derived relationship to set the concentration of silt entering
629 the domain at the upstream boundary of our model runs.

630 **Acknowledgements**

631 This work was supported by National Science Foundation grant 1812019, National Science
632 Foundation grant, 1426997, and National Science Foundation grant 1135427. All data will be
633 made available upon publication through the IU ScholarWorks repository
634 <http://scholarworks.iu.edu>. We could like to thank Deon Knights for assistance with field work
635 and the Coastal Systems Ecology Lab at Louisiana State University for access to data collected
636 by observation platforms located in the Wax Lake Delta and maintenance of said platforms.

637 **Citations**

- 638 Allison, M. A., Demas, C. R., Ebersole, B. A., Kleiss, B. A., Little, C. D., Meselhe, E. A., ... &
639 Vosburg, B. M. (2012). A water and sediment budget for the lower Mississippi–
640 Atchafalaya River in flood years 2008–2010: implications for sediment discharge to the
641 oceans and coastal restoration in Louisiana. *Journal of Hydrology*, 432, 84-97.
- 642 Allison, M. A., Yuill, B. T., Meselhe, E. A., Marsh, J. K., Kolker, A. S., & Ameen, A. D. (2017).
643 Observational and numerical particle tracking to examine sediment dynamics in a
644 Mississippi River delta diversion. *Estuarine, Coastal and Shelf Science*, 194, 97-108.
- 645 Baptist, M. J. (2005). Modelling floodplain biogeomorphology.
- 646 Bevington, A. E., Twilley, R. R., Sasser, C. E., & Holm Jr, G. O. (2017). Contribution of river
647 floods, hurricanes, and cold fronts to elevation change in a deltaic floodplain, northern
648 Gulf of Mexico, USA. *Estuarine, Coastal and Shelf Science*, 191, 188-200.
- 649 Blum, M. D., & Roberts, H. H. (2009). Drowning of the Mississippi Delta due to insufficient
650 sediment supply and global sea-level rise. *Nature Geoscience*, 2(7), 488.

- 651 Carle, M. V., Sasser, C. E., & Roberts, H. H. (2015). Accretion and vegetation community
652 change in the Wax Lake Delta following the historic 2011 Mississippi River
653 flood. *Journal of Coastal Research*, 31(3), 569-587.
- 654 Childers, D. L., & Day, J. W. (1990). Marsh-water column interactions in two Louisiana
655 estuaries. I. Sediment dynamics. *Estuaries*, 13(4), 393-403.
- 656 Christiansen, T., Wiberg, P. L., & Milligan, T. G. (2000). Flow and sediment transport on a tidal
657 salt marsh surface. *Estuarine, Coastal and Shelf Science*, 50(3), 315-331.
- 658 Couvillion, B. R., Barras, J. A., Steyer, G. D., Sleavin, W., Fischer, M., Beck, H., ... & Heckman,
659 D. (2011). Land area change in coastal Louisiana from 1932 to 2010.
- 660 CPRA. (2017). Louisiana's Comprehensive Master Plan for a Sustainable Coast. Coastal
661 Protection and Restoration Authority of Louisiana, Baton Rouge, LA. pp. 171.
- 662 Day, J. W., Britsch, L. D., Hawes, S. R., Shaffer, G. P., Reed, D. J., & Cahoon, D. (2000).
663 Pattern and process of land loss in the Mississippi Delta: a spatial and temporal analysis
664 of wetland habitat change. *Estuaries*, 23(4), 425-438.
- 665 Day, J. W., Boesch, D. F., Clairain, E. J., Kemp, G. P., Laska, S. B., Mitsch, W. J., ... &
666 Simenstad, C. A. (2007). Restoration of the Mississippi Delta: lessons from hurricanes
667 Katrina and Rita. *science*, 315(5819), 1679-1684.
- 668 Day, J. W., Kemp, G. P., Reed, D. J., Cahoon, D. R., Boumans, R. M., Suhayda, J. M., &
669 Gambrell, R. (2011). Vegetation death and rapid loss of surface elevation in two
670 contrasting Mississippi delta salt marshes: The role of sedimentation, autocompaction
671 and sea-level rise. *Ecological Engineering*, 37(2), 229-240.
- 672
- 673 Day, J., Cable, J., Lane, R., & Kemp, G. (2016a). Sediment deposition at the Caernarvon
674 crevasse during the great Mississippi flood of 1927: implications for coastal
675 restoration. *Water*, 8(2), 38.
- 676 Day, J. W., Agboola, J., Chen, Z., D'Elia, C., Forbes, D. L., Giosan, L., ... & Syvitski, J. (2016b).
677 Approaches to defining deltaic sustainability in the 21st century. *Estuarine, coastal and
678 shelf science*, 183, 275-291.
- 679 Denes, T. A., & Caffrey, J. M. (1988). Changes in seasonal water transport in a Louisiana
680 estuary, Fourleague Bay, Louisiana. *Estuaries*, 11(3), 184-191.
- 681 Esposito, C. R., Georgiou, I. Y., & Kolker, A. S. (2013). Hydrodynamic and geomorphic
682 controls on mouth bar evolution. *Geophysical Research Letters*, 40(8), 1540-1545.
- 683 Esposito, C. R., Shen, Z., Törnqvist, T. E., Marshak, J., & White, C. (2017). Efficient retention
684 of mud drives land building on the Mississippi Delta plain. *Earth Surface
685 Dynamics*, 5(3), 387-397.
- 686 Fabre, J. B. (2012). Sediment flux & fate for a large-scale diversion: the 2011 Mississippi River
687 Flood, the Bonnet Carré Spillway, and the implications for coastal restoration in south
688 Louisiana.

- 689 Fagherazzi, S., Kirwan, M. L., Mudd, S. M., Guntenspergen, G. R., Temmerman, S., D'Alpaos,
690 A., ... & Clough, J. (2012). Numerical models of salt marsh evolution: Ecological,
691 geomorphic, and climatic factors. *Reviews of Geophysics*, 50(1).
- 692 Ferguson, R. I., & Church, M. (2004). A simple universal equation for grain settling
693 velocity. *Journal of sedimentary Research*, 74(6), 933-937.
- 694 Gagliano, S. M., Meyer-Arendt, K. J., & Wicker, K. M. (1981). Land loss in the Mississippi
695 River deltaic plain.
- 696 Gedan, K. B., Kirwan, M. L., Wolanski, E., Barbier, E. B., & Silliman, B. R. (2011). The present
697 and future role of coastal wetland vegetation in protecting shorelines: answering recent
698 challenges to the paradigm. *Climatic Change*, 106(1), 7-29.
- 699 Geleynse, N., Hiatt, M., Sangireddy, H., & Passalacqua, P. (2015). Identifying environmental
700 controls on the shoreline of a natural river delta. *Journal of Geophysical Research: Earth
701 Surface*, 120(5), 877-893.
- 702 Grace, J. B. (1989). Effects of water depth on *Typha latifolia* and *Typha domingensis*. *American
703 Journal of Botany*, 76(5), 762-768.
- 704 Hiatt, M., Snedden, G., Day, J. W., Rohli, R. V., Nyman, J. A., Lane, R., & Sharp, L. A. (2019).
705 Drivers and impacts of water level fluctuations in the Mississippi River delta:
706 Implications for delta restoration. *Estuarine, Coastal and Shelf Science*, 224, 117-137.
- 707 Hoitink, A. J. F., & Jay, D. A. (2016). Tidal river dynamics: Implications for deltas. *Reviews of
708 Geophysics*, 54(1), 240-272.
- 709 Howes, N. C., FitzGerald, D. M., Hughes, Z. J., Georgiou, I. Y., Kulp, M. A., Miner, M. D., ... &
710 Barras, J. A. (2010). Hurricane-induced failure of low salinity wetlands. *Proceedings of
711 the National Academy of Sciences*, 107(32), 14014-14019.
- 712 Kadlec, R. H., & Wallace, S. (2008). *Treatment wetlands*. CRC press.
- 713 Keogh, M. E., Kolker, A. S., Snedden, G. A., & Renfro, A. A. (2019). Hydrodynamic controls on
714 sediment retention in an emerging diversion-fed delta. *Geomorphology*, 332, 100-111.
- 715 Kim, W., Mohrig, D., Twilley, R., Paola, C., & Parker, G. (2009). Is it feasible to build new land
716 in the Mississippi River Delta?. *Eos, Transactions American Geophysical Union*, 90(42),
717 373-374.
- 718 Kirwan, M. L., & Murray, A. B. (2007). A coupled geomorphic and ecological model of tidal
719 marsh evolution. *Proceedings of the National Academy of Sciences*, 104(15), 6118-6122.
- 720 Kleinhans, M. G., de Vries, B., Braat, L., & van Oorschot, M. (2018). Living landscapes: Muddy
721 and vegetated floodplain effects on fluvial pattern in an incised river. *Earth surface
722 processes and landforms*, 43(14), 2948-2963.
- 723 Kolker, A. S., Miner, M. D., & Weathers, H. D. (2012). Depositional dynamics in a river
724 diversion receiving basin: The case of the West Bay Mississippi River
725 Diversion. *Estuarine, Coastal and Shelf Science*, 106, 1-12.

- 726 Lane, E. M., Restrepo, J. M., & McWilliams, J. C. (2007). Wave–current interaction: A
727 comparison of radiation-stress and vortex-force representations. *Journal of physical*
728 *oceanography*, 37(5), 1122-1141.
- 729 Larsen, L. G. (2019). Multiscale flow-vegetation-sediment feedbacks in low-gradient
730 landscapes. *Geomorphology*.
- 731 Leonard, L. A., & Luther, M. E. (1995). Flow hydrodynamics in tidal marsh canopies.
732 *Limnology and oceanography*, 40(8), 1474-1484.
- 733 Ma, H., Larsen, L. G., & Wagner, R. W. (2018). Ecogeomorphic Feedbacks that Grow
734 Deltas. *Journal of Geophysical Research: Earth Surface*, 123(12), 3228-3250.
- 735 Madden, C. J., Day Jr, J. W., & Randall, J. M. (1988). Freshwater and marine coupling in
736 estuaries of the Mississippi River deltaic plain 1. *Limnology and*
737 *Oceanography*, 33(4part2), 982-1004.
- 738 Mariotti, G. (2016). Revisiting salt marsh resilience to sea level rise: Are ponds responsible for
739 permanent land loss?. *Journal of Geophysical Research: Earth Surface*, 121(7), 1391-
740 1407.
- 741 Meade, R. H., & Moody, J. A. (2010). Causes for the decline of suspended-sediment discharge in
742 the Mississippi River system, 1940–2007. *Hydrological Processes: An International*
743 *Journal*, 24(1), 35-49.
- 744 Miller, R. L., & Fujii, R. (2010). Plant community, primary productivity, and environmental
745 conditions following wetland re-establishment in the Sacramento-San Joaquin Delta,
746 California. *Wetlands Ecology and Management*, 18(1), 1-16.
- 747 Morris, J. T., Sundareshwar, P. V., Nietch, C. T., Kjerfve, B., & Cahoon, D. R. (2002).
748 Responses of coastal wetlands to rising sea level. *Ecology*, 83(10), 2869-2877.
- 749 Nardin, W., & Edmonds, D. A. (2014). Optimum vegetation height and density for inorganic
750 sedimentation in deltaic marshes. *Nature Geoscience*, 7(10), 722.
- 751 Nardin, W., Edmonds, D. A., & Fagherazzi, S. (2016). Influence of vegetation on spatial patterns
752 of sediment deposition in deltaic islands during flood. *Advances in Water Resources*, 93,
753 236-248.
- 754 Neumeier, U., & Ciavola, P. (2004). Flow resistance and associated sedimentary processes in a
755 *Spartina maritima* salt-marsh. *Journal of Coastal Research*, 435-447.
- 756 NOAA (2011). USGS Atchafalaya 2 LiDAR. NOAA’s Ocean Service, Office for Coastal
757 Management (OCM), Charleston, SC.
- 758 Olliver, E. A., & Edmonds, D. A. (2017). Defining the ecogeomorphic succession of land
759 building for freshwater, intertidal wetlands in Wax Lake Delta, Louisiana. *Estuarine,*
760 *Coastal and Shelf Science*, 196, 45-57.
- 761 Ortiz, A. C., Roy, S., & Edmonds, D. A. (2017). Land loss by pond expansion on the Mississippi
762 River Delta Plain. *Geophysical Research Letters*, 44(8), 3635-3642.

- 763 Paola, C., Twilley, R. R., Edmonds, D. A., Kim, W., Mohrig, D., Parker, G., ... & Voller, V. R.
764 (2011). Natural processes in delta restoration: Application to the Mississippi
765 Delta. *Annual review of marine science*, 3, 67-91.
- 766 Partheniades, E. (1965). Erosion and deposition of cohesive soils. *Journal of the Hydraulics*
767 *Division*, 91(1), 105-139.
- 768 Perez, B. C., Day Jr, J. W., Rouse, L. J., Shaw, R. F., & Wang, M. (2000). Influence of
769 Atchafalaya River discharge and winter frontal passage on suspended sediment
770 concentration and flux in Fourleague Bay, Louisiana. *Estuarine, Coastal and Shelf*
771 *Science*, 50(2), 271-290.
- 772
- 773 Peyronnin, N., Caffey, R., Cowan, J., Justic, D., Kolker, A., Laska, S., ... & Visser, J. (2017).
774 Optimizing sediment diversion operations: working group recommendations for
775 integrating complex ecological and social landscape interactions. *Water*, 9(6), 368.
- 776 Roberts, H. H., Coleman, J. M., Bentley, S. J., & Walker, N. (2003). An embryonic major delta
777 lobe: A new generation of delta studies in the Atchafalaya-Wax Lake Delta system.
- 778 Rosen, T., & Xu, Y. J. (2013). Recent decadal growth of the Atchafalaya River Delta complex:
779 Effects of variable riverine sediment input and vegetation succession. *Geomorphology*,
780 194, 108-120.
- 781 Rosenheim, B. E., Roe, K. M., Roberts, B. J., Kolker, A. S., Allison, M. A., & Johannesson, K.
782 H. (2013). River discharge influences on particulate organic carbon age structure in the
783 Mississippi/Atchafalaya River System. *Global Biogeochemical Cycles*, 27(1), 154-166.
- 784 Sendrowski, A., & Passalacqua, P. (2017). Process connectivity in a naturally prograding river
785 delta. *Water Resources Research*, 53(3), 1841-1863.
- 786 Shaw, J. B., Mohrig, D., & Whitman, S. K. (2013). The morphology and evolution of channels
787 on the Wax Lake Delta, Louisiana, USA. *Journal of Geophysical Research: Earth*
788 *Surface*, 118(3), 1562-1584.
- 789 Shaw, J. B., Ayoub, F., Jones, C. E., Lamb, M. P., Holt, B., Wagner, R. W., ... & Mohrig, D.
790 (2016). Airborne radar imaging of subaqueous channel evolution in Wax Lake Delta,
791 Louisiana, USA. *Geophysical Research Letters*, 43(10), 5035-5042.
- 792 Shen, Z., Törnqvist, T. E., Mauz, B., Chamberlain, E. L., Nijhuis, A. G., & Sandoval, L. (2015).
793 Episodic overbank deposition as a dominant mechanism of floodplain and delta-plain
794 aggradation. *Geology*, 43(10), 875-878.
- 795 Smith, J. E., Bentley, S. J., Snedden, G. A., & White, C. (2015). What role do hurricanes play in
796 sediment delivery to subsiding river deltas?. *Scientific reports*, 5, 17582.
- 797 Snedden, G. A., Cable, J. E., Swarzenski, C., & Swenson, E. (2007). Sediment discharge into a
798 subsiding Louisiana deltaic estuary through a Mississippi River diversion. *Estuarine,*
799 *Coastal and Shelf Science*, 71(1-2), 181-193.

- 800 Stanley, D. J., & Warne, A. G. (1993). Nile Delta: recent geological evolution and human
801 impact. *Science*, 260(5108), 628-634.
- 802 Stern, M. K., Day, J. W., & Teague, K. G. (1991). Nutrient transport in a riverine-influenced,
803 tidal freshwater bayou in Louisiana. *Estuaries*, 14(4), 382-394.
- 804 Stumpf, R. P. (1983). The process of sedimentation on the surface of a salt marsh. *Estuarine,
805 Coastal and Shelf Science*, 17(5), 495-508.
- 806 Syvitski, J. P., Vörösmarty, C. J., Kettner, A. J., & Green, P. (2005). Impact of humans on the
807 flux of terrestrial sediment to the global coastal ocean. *science*, 308(5720), 376-380.
- 808 Syvitski, J. P., & Saito, Y. (2007). Morphodynamics of deltas under the influence of
809 humans. *Global and Planetary Change*, 57(3-4), 261-282.
- 810 Temmerman, S., Bouma, T. J., Govers, G., Wang, Z. B., De Vries, M. B., & Herman, P. M. J.
811 (2005). Impact of vegetation on flow routing and sedimentation patterns: Three-
812 dimensional modeling for a tidal marsh. *Journal of Geophysical Research: Earth
813 Surface*, 110(F4).
- 814 Temmerman, S., Bouma, T. J., Van de Koppel, J., Van der Wal, D., De Vries, M. B., & Herman,
815 P. M. J. (2007). Vegetation causes channel erosion in a tidal landscape. *Geology*, 35(7),
816 631-634.
- 817 Turner, R. E., Baustian, J. J., Swenson, E. M., & Spicer, J. S. (2006). Wetland sedimentation
818 from hurricanes Katrina and Rita. *Science*, 314(5798), 449-452.
- 819 Van Heerden, I. L., & Roberts, H. H. (1988). Facies development of Atchafalaya Delta,
820 Louisiana: a modern bayhead delta. *AAPG Bulletin*, 72(4), 439-453.
- 821 Wang, J., Xu, K., Restrepo, G. A., Bentley, S. J., Meng, X., & Zhang, X. (2018). The coupling
822 of bay hydrodynamics to sediment transport and its implication in micro-tidal wetland
823 sustainability. *Marine Geology*, 405, 68-76.
- 824 Weerman, E. J., Van Belzen, J., Rietkerk, M., Temmerman, S., Kéfi, S., Herman, P. M. J., & de
825 Koppel, J. V. (2012). Changes in diatom patch-size distribution and degradation in a
826 spatially self-organized intertidal mudflat ecosystem. *Ecology*, 93(3), 608-618.
- 827 Wright, L. D., & Coleman, J. M. (1972). River delta morphology: wave climate and the role of
828 the subaqueous profile. *Science*, 176(4032), 282-284.
- 829 Wright, L. D., & Coleman, J. M. (1973). Variations in morphology of major river deltas as
830 functions of ocean wave and river discharge regimes. *AAPG Bulletin*, 57(2), 370-398.
- 831 Wright, L. D. (1977). Sediment transport and deposition at river mouths: a synthesis. *Geological
832 Society of America Bulletin*, 88(6), 857-868.
- 833 Xing, F., Syvitski, J. P., Kettner, A. J., Meselhe, E. A., Atkinson, J. H., & Khadka, A. K. (2017).
834 Morphological responses of the Wax Lake Delta, Louisiana, to Hurricanes
835 Rita. *Elementa Science of the Anthropocene*.
- 836 Xu, K., Bentley, S. J., Day, J. W., & Freeman, A. M. (2019). A review of sediment diversion in
837 the Mississippi River Deltaic Plain. *Estuarine, Coastal and Shelf Science*.

- 838 Yamasaki, T. N., de Lima, P. H., Silva, D. F., Cristiane, G. D. A., Janzen, J. G., & Nepf, H. M.
839 (2019). From patch to channel scale: The evolution of emergent vegetation in a
840 channel. *Advances in Water Resources*, 129, 131-145.
- 841 Yang, S. L., Zhang, J., Zhu, J., Smith, J. P., Dai, S. B., Gao, A., & Li, P. (2005). Impact of dams
842 on Yangtze River sediment supply to the sea and delta intertidal wetland
843 response. *Journal of Geophysical Research: Earth Surface*, 110(F3).
- 844 Yang, S. L., Li, H., Ysebaert, T., Bouma, T. J., Zhang, W. X., Wang, Y. Y., ... & Ding, P. X.
845 (2008). Spatial and temporal variations in sediment grain size in tidal wetlands, Yangtze
846 Delta: On the role of physical and biotic controls. *Estuarine, Coastal and Shelf
847 Science*, 77(4), 657-671.